CHINESE JOURNAL OF PHYSICS VOL. 39, NO. 1 FEBRUARY 2001

Effects of Incoherent Processes on the Quantum Transport through a Finite-range Time-modulated Potential

H. C. Liang and C. S. Chu

Department of Electrophysics, National Chiao Tung University, Hsinchu, Taiwan 300, R.O.C.

(Received June 21, 2000)

We study the effect of phase randomization on the quantum transport through a finite-range time-modulated potential. The time-modulated potential leads only to coherent inelastic scatterings, and the incoherent processes are described by an S-matrix model proposed originally by Büttiker for the case of time-independent transport. This S-matrix model provides us a systematic way to reinject into the system those electrons that have suffered with incoherent scatterings. The distribution of these reinjected electrons is determined by an effective chemical potential μ. For comparison, we study the cases where the incoherent processes occur inside and outside the time-modulated region. The incoherent processes are found to broaden and to smear the structures in the conductance G that are associated with the coherent inelastic scatterings. However, the smearing is more effective when the incoherent processes occur inside the time-modulated potential region.

PACS. 72.10.–d – Theory of electronic transport; scattering mechanisms.
PACS. 72.40.+w – Photoconduction and photovoltaic effects.
PACS. 73.40.–c – Electronic transport in interface structures.

I. Introduction

The effects of phase randomization on the quantum transport have drawn continuous attention in the recent past. These studies are usually related to inelastic scatterings [1-4]. But inelastic scattering does not necessarily lead to incoherence. There are coherent inelastic scatterings [5, 6], when the system of interest is acted upon by an externally specified time-modulated field. On the other hand, there are decoherence effects resulting from collisions leading to large energy transfer. More recently, decoherence effects resulted from small energy transfer collisions are recognized [7]. The environment from which the systems are scattered incoherently consists of many degrees of freedom.

In this work we do not explore the microscopic mechanisms for dephasing; rather, we explore qualitatively the possible effects of dephasing on our system of interest. Since there is as yet no simple microscopic approach for the implementation of the incoherent processes, our choices are left with two widely used models for our qualitative exploration. One of the models is an S-matrix model, proposed by Büttiker [8], that consists of a coupler coupling the incoherently scattered electrons to a reservoir from which these particles will be reinjected back into the system. The distribution of the reinjected electrons is given by the effective chemical potential μ of the reservoir. There is no phase correlation between the electrons entering and leaving the reservoir,

and this leads to the lost in the phases of these electrons in the system. Another model invokes a complex potential [2-3]. In this model the wavevector is complex and the wavefunctions become attenuated, in accordance with the inelastic mean free path. This attenuation in the wavefunction reflects the nonconservation of the particle in the system and also that the Hamiltonian is non-Hermitian. Basically, the model only keeps track of the coherent part of the wavefunction. A direct comparison of these two models have been made recently for the case of a conducting ring threaded by a magnetic flux [9]. The S-matrix model was shown to produce results more consistent with the symmetry in two-probe magneto-conductance experiments.

We thus choose the S-matrix model for the incoherent processes in our systems and we extend it to the case when the system is acted upon by a time-modulated potential. The system we consider is a narrow constriction (NC) connected adiabatically to two end-electrodes. In this system, the effect of a finite-range time-modulated potential on the coherent inelastic transport was studied recently [6]. It was found that the transmitting electrons can be trapped temporarily within the time-modulated region if they can make intersideband transitions to their subband bottom by emitting $n\sim!$. The electrons are trapped by quasibound states induced by the time-modulated potential. The existence of these quasibound states depends on the singular density of states at a subband bottom. These quasibound states were found to exhibit interesting dip structures in the dc conductance G [6]. Since only coherent inelastic scatterings were considered and the incoherent processes were assumed to occur only in the two end-electrodes [6], it is legitimate to explore the effects, to these interesting G structures, of incoherent scatterings that occur in the time-modulated region.

In Sec. II we present our formulation that treats the coherent inelastic scattering and the incoherent scattering nonperturbatively, and on the same footing. Both the cases that incoherent scattering occurs either inside or outside the region of the time-modulated potential are investigated. We calculate the dc conductance G in the low source-drain bias regime. In Sec. III numerical examples illustrating the influence of incoherent scatterings to the structures in G will be presented. Finally, Sec. IV presents a conclusion.

II. Theory

In this section, we outline our formulation that treats the inelastic and the incoherent scatterings nonperturbatively and on the same footing. Even though the NC is assumed to be one dimensional in this work, the formulation is readily to be generalized to multi-channel cases. We expect, however, that the one channel NC has already captured the essential physics for the inelastic scatterings. The NC is acted upon by a time-modulated potential of the form

$$V(x;t) = V\cos(!t)\mu(L=2 ¡ jxj); \tag{1}$$

where L is the spatial extent of the potential and x is the propagation direction. With a convenient choice of units: energy unit $E^{\alpha} = \sim^2 k_F^2/2m^{\alpha}$; length unit $a^{\alpha} = 1/k_F$; time unit $t^{\alpha} = \sim/E^{\alpha}$; and k_F a typical Fermi wavevector for the system, the Schrödinger equation can be converted into its dimensionless form, given by

$$¡\frac{@^2}{@x^2} + V(x;t)\Big]^{a}(x;t) = i\frac{@}{@t}{}^{a}(x;t): \tag{2}$$

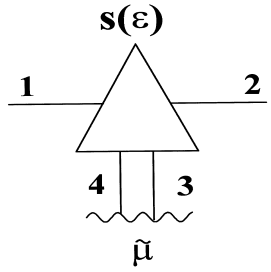

FIG. 1. Sketch of an incoherent scatterer. This scatterer consists of a S-matrix coupler, denoted by the triangle, and a reservoir μ. The four connecting leads are indicated in the same figure.

Here m^* is the effective mass of the electrons.

The incoherent process that occurs in NC is represented by a S-matrix, as shown in Fig. 1, that connects to NC, via leads 1 and 2, and also to a reservoir, via leads 3 and 4. As mentioned earlier, the purpose of this reservoir is to facilitate the removal of phase coherence from electrons entering it. The chemical potential μ of the reservoir defines the distribution of the electrons leaving the reservoir, and its value is chosen such that the net current between the reservoir and NC is zero. An explicit form for the unitary S-matrix $S(\varepsilon)$ is given by [8]

$$S(\varepsilon) = \begin{bmatrix} 0 & \sqrt{1-\varepsilon} & \sqrt{\varepsilon} & 0 \\ \sqrt{1-\varepsilon} & 0 & 0 & \sqrt{\varepsilon} \\ \sqrt{\varepsilon} & 0 & 0 & -i\sqrt{1-\varepsilon} \\ 0 & \sqrt{\varepsilon} & -i\sqrt{1-\varepsilon} & 0 \end{bmatrix}; \tag{3}$$

which connects incoming waves, with amplitudes $a = (a_1; a_2; a_3; a_4)$, to the outgoing waves, with amplitudes $b = (b_1; b_2; b_3; b_4)$, through the relation

$$b^T = S(\varepsilon)a^T: \tag{4}$$

The coupling parameter ε in $S(\varepsilon)$ ranges between $0 \cdot \varepsilon \cdot 1$ and denotes the extent the NC couples with the reservoir. For $\varepsilon = 1$, the electron will lose track of its phase entirely once it encounters the coupler. For $\varepsilon = 0$, the NC and the reservoir μ are decoupled. The form of $S(\varepsilon)$ is chosen such that the diagonal matrix element is zero. By this choice, the S-matrix does not produce back-scattering. Hence the model has a nice feature that the outgoing amplitudes do not depend on the location of this incoherent scatterer. Furthermore, even though we have chosen the $S(\varepsilon)$ coupler to locate at $x = x_0$, our result would not depend on the specific values of x_0. However, our result would depend on whether x_0 is inside or outside the time-modulated region.

II-1. Incoherent scatterings inside the time-modulated region

We first consider the case that the $S(\varepsilon)$ coupler locates inside the time-modulated region. The electron can incident from the left reservoir via lead 1, or the right reservoir via lead 2, or from the reservoir associated with the coupler via leads 3 or 4. The resulting scattering states ψ^+_m,

with m ranges from 1 to 4 and indicates the incident lead, can be written in the form [4, 5]

$$a_m^+ = \begin{cases} \sum_n [\pm_{m;1}\pm_{n;0} e^{iq_n(x+\frac{L}{2})} + t_{m1n} e^{-iq_n(x+\frac{L}{2})}] e^{-i(E+n\omega)t} & x < -L/2 \\ \sum_n [\alpha_{m1n} e^{iq_n x} + \beta_{m1n} e^{-iq_n x}] e^{-i(E+n\omega)t} \sum_l J_l(V/\omega) e^{-il\omega t} & -L/2 < x < x_0 \\ \sum_n [\alpha_{m2n} e^{-iq_n x} + \beta_{m2n} e^{iq_n x}] e^{-i(E+n\omega)t} \sum_l J_l(V/\omega) e^{-il\omega t} & x_0 < x < L/2 \\ \sum_n [\pm_{m;2}\pm_{n;0} e^{-iq_n(x-\frac{L}{2})} + t_{m2n} e^{iq_n(x-\frac{L}{2})}] e^{-i(E+n\omega)t} & x > L/2 \\ \sum_n [\pm_{m;3}\pm_{n;0} e^{iq_n y} + \beta_{m3n} e^{-iq_n y}] e^{-i(E+n\omega)t} \sum_l J_l(V/\omega) e^{-il\omega t} & \text{lead } 3; y < 0 \\ \sum_n [\pm_{m;4}\pm_{n;0} e^{iq_n y} + \beta_{m4n} e^{-iq_n y}] e^{-i(E+n\omega)t} \sum_l J_l(V/\omega) e^{-il\omega t} & \text{lead } 4; y < 0. \end{cases} \tag{5}$$

Here, y is the coordinate in leads 3 and 4 with the coupler located at $y = 0$. The symbol n is an integer indicating the nth sideband such that it corresponds to an energy $E + n\omega$ in the wavefunction outside the time-modulated region, where $|x| > L/2$. The coefficients α_{min} and β_{min} represent incoming and outgoing amplitudes, respectively, in lead i that connects to the incoherent scatterer. The coefficients t_{m1n} and t_{m2n} represent amplitudes leaving the time-modulated region and approaching reservoirs 1 and 2 respectively. The effective wavevector for an electron in the nth-sideband is $q_n = \sqrt{E + n\omega}$. Finally, the above wavefunction in the time-modulated region consists of a factor that involves a summation over l. This follows from the identity $e^{-i\frac{V}{\omega}\sin\omega t} = \sum_l J_l(\frac{V}{\omega}) e^{-il\omega t}$. The expressions for the reflection and transmission coefficients can be obtained from matching the wavefunctions and their derivatives at $x = \pm L/2$, and at all times. For the matching at the coupler, we use Eq. (3) and obtain

$$\begin{cases} \beta_{m1n} = \sqrt{1-\varepsilon}\,\alpha_{m2n} + \sqrt{\varepsilon}\,\pm_{m;3}\pm_{n;0} e^{iq_n x_0} \\ \beta_{m2n} = \sqrt{1-\varepsilon}\,\alpha_{m1n} + \sqrt{\varepsilon}\,\pm_{m;4}\pm_{n;0} e^{iq_n x_0} \\ \beta_{m3n} = \sqrt{\varepsilon}\,\alpha_{m1n} e^{iq_n x_0} - \sqrt{1-\varepsilon}\,\pm_{m;4}\pm_{n;0} \\ \beta_{m4n} = \sqrt{\varepsilon}\,\alpha_{m2n} e^{-iq_n x_0} - \sqrt{1-\varepsilon}\,\pm_{m;3}\pm_{n;0}. \end{cases} \tag{6}$$

The matching at $x = \pm L/2$ gives us

$$\begin{cases} t_{m1n} + \pm_{m;1}\pm_{n;0} = \sum_l J_{n-l}(V/\omega) \left[\beta_{m1l} e^{iq_l\frac{L}{2}} + \alpha_{m1l} e^{-iq_l\frac{L}{2}}\right] \\ t_{m1n} - \pm_{m;1}\pm_{n;0} = \sum_l \frac{q_l}{q_n} J_{n-l}(V/\omega) \left[\beta_{m1l} e^{iq_l\frac{L}{2}} - \alpha_{m1l} e^{-iq_l\frac{L}{2}}\right] \\ t_{m2n} + \pm_{m;2}\pm_{n;0} = \sum_l J_{n-l}(V/\omega) \left[\beta_{m2l} e^{iq_l\frac{L}{2}} + \alpha_{m2l} e^{-iq_l\frac{L}{2}}\right] \\ t_{m2n} - \pm_{m;2}\pm_{n;0} = \sum_l \frac{q_l}{q_n} J_{n-l}(V/\omega) \left[\beta_{m2l} e^{iq_l\frac{L}{2}} - \alpha_{m2l} e^{-iq_l\frac{L}{2}}\right]. \end{cases} \tag{7}$$

We solve the above equations numerically for the coefficients. The correctness of our results is checked against the conservation of current for each incident electron. The condition is given by

$$\sum_n{}' \frac{q_n}{q_0}\left(|t_{m1n}|^2 + |t_{m2n}|^2 + |r_{m3n}|^2 + |r_{m4n}|^2\right) = 1. \tag{8}$$

The above summation, indicated by the primed superscript, includes only the propagating modes. It can be shown from simplifying Eqs. (6) and (7) that x_0 appears only as an overall phase factor to the coefficients. This trivial dependence on x_0 is elliminated automatically from all physical quantities, such as the current through the structure.

After we solve the above equations for the coefficients, we can apply them to the calculation of the currents in all the leads for a given set of chemical potentials μ_1, μ_2, and μ. Here μ_1, μ_2 are the chemical potentials for reservoirs 1 and 2, respectively. For a given bias, with $\mu_1 = \mu + \pm\mu$ and $\mu_2 = \mu$, we have to adjust μ such that there is no net current between the reservoir μ and NC. It is convenient to define $\mu = \mu_0 + \pm\mu$, where μ_0 is determined from the case of zero bias (i.e. $\pm\mu = 0$) between leads 1 and 2. The determination of $\pm\mu$ for the low bias case is quite straightforward, according to the following procedure.

First of all, to determine μ_0, the total current in leads 3 and 4, denoted by $I_3(\mu;\mu_0) + I_4(\mu;\mu_0)$, must be zero. But the symmetry of the structure gives $I_3(\mu;\mu_0) = I_4(\mu;\mu_0)$. Therefore the condition becomes $I_3(\mu;\mu_0) = 0$. The current in lead 3 has contribution coming from electrons in reservoirs 1 and 2, given by

$$I_3^{1;2}(\mu) = \frac{2e}{h}\int_0^{\mu} dE \sum_n \frac{q_n}{q_0}\left(|r_{13n}|^2 + |r_{23n}|^2\right); \tag{9}$$

and from electrons in reservoirs 3 and 4, given by

$$I_3^{3;4}(\mu_0) = \frac{2e}{h}\int_0^{\mu_0} dE \left[\sum_n \frac{q_n}{q_0}\left(|r_{33n}|^2 + |r_{43n}|^2\right) - 1\right]. \tag{10}$$

Hence μ_0 can be determined from requiring $I_3^{1;2}(\mu) = -I_3^{3;4}(\mu_0)$.

Now, in the low-bias regime, when $\pm\mu$ is very small, the total change in the current $\pm I_3 + \pm I_4$ must still be zero. This can be achieved by adjusting μ_0 to $\mu_0 + \pm\mu$. The condition becomes

$$\begin{aligned} \pm I_3 + \pm I_4 &= -\frac{2e\pm\mu}{h}\left[2\sum_{n(\mu_0)} \frac{q_n}{q_0}\left(|r_{33n}|^2 + |r_{34n}|^2 + |r_{43n}|^2 + |r_{44n}|^2\right)\right] \\ &\quad + \frac{2e\pm\mu}{h}\sum_{n(\mu)} \frac{q_n}{q_0}\left(|r_{13n}|^2 + |r_{14n}|^2\right) \\ &= 0. \end{aligned} \tag{11}$$

Consequently, we obtain the relation between $\pm\mu$ and $\pm\mu$, given by

$$\pm\mu = \frac{\sum_{n(\mu)} \frac{q_n}{q_0}\left(|r_{13n}|^2 + |r_{14n}|^2\right)}{\sum_{n(\mu_0)} \frac{q_n}{q_0}\left(|r_{33n}|^2 + |r_{34n}|^2 + |r_{43n}|^2 + |r_{44n}|^2\right)}\pm\mu; \tag{12}$$

where the symbols $n(\epsilon)$, or $n(\epsilon_0)$, in the summations indicate evaluation at energies ϵ, or ϵ_0, respectively.

The zero-temperature conductance G is then given by

$$G = \frac{\pm I_2}{(\pm^1/e)} = \frac{2e^2}{h}\left\{\sum_{n(\epsilon)} \frac{q_n}{q_0}|t_{12n}|^2 + \frac{\left[\sum_{n(\epsilon)} \frac{q_n}{q_0}(|\bar{}_{13n}|^2 + |\bar{}_{14n}|^2)\right]\left[\sum_{n(\epsilon_0} \frac{q_n}{q_0}(|t_{32n}|^2 + |t_{42n}|^2)\right]}{2 - \sum_{n(\epsilon_0)} \frac{q_n}{q_0}(|\bar{}_{33n}|^2 + |\bar{}_{34n}|^2 + |\bar{}_{43n}|^2 + |\bar{}_{44n}|^2)}\right\}. \tag{13}$$

It can also be shown equal to

$$G = \frac{-\pm I_1}{(\pm^1/e)} = \frac{2e^2}{h}\left\{1 - \sum_{n(\epsilon)} \frac{q_n}{q_0}|t_{11n}|^2 - \frac{\left[\sum_{n(\epsilon)} \frac{q_n}{q_0}(|\bar{}_{13n}|^2 + |\bar{}_{14n}|^2)\right]\left[\sum_{n(\epsilon_0)} \frac{q_n}{q_0}(|t_{31n}|^2 + |t_{41n}|^2)\right]}{2 - \sum_{n(\epsilon_0)} \frac{q_n}{q_0}(|\bar{}_{33n}|^2 + |\bar{}_{34n}|^2 + |\bar{}_{43n}|^2 + |\bar{}_{44n}|^2)}\right\}. \tag{14}$$

II-2. Incoherent scatterings outside the time-modulated region

For the purpose of comparing with the results in the previous subsection, we consider here the case when the S(") coupler locates outside the time-modulated region. Without lose of generality, we let $x_0 < -L/2$. The scattering states a^+_m can be written in the form

$$a^+_m = \begin{cases} \sum_n \left[\pm_{m;1}\pm_{n;0}e^{iq_n(x-x_0)} + \bar{}_{m1n}e^{-iq_n(x-x_0)}\right]e^{-i(E+n!)t} & x < x_0 \\ \sum_n \left[\circledR_{m2n}e^{-iq_n(x-x_0)} + \bar{}_{m2n}e^{iq_n(x-x_0)}\right]e^{-i(E+n!)t} & x_0 < x < -L/2 \\ \sum_n \left[c_{mn}e^{iq_n(x+\frac{L}{2})} + d_{mn}e^{-iq_n(x+\frac{L}{2})}\right]e^{-i(E+n!)t}\sum_l J_l(V/!)e^{-il!t} & |x| < L/2 \\ \sum_n \left[\pm_{m;2}\pm_{n;0}e^{iq_n(x-\frac{L}{2})} + t_{m2n}e^{iq_n(x-\frac{L}{2})}\right]e^{-i(E+n!)t} & x > L/2 \\ \sum_n \left\{\pm_{m;3}\pm_{n;0}e^{iq_n y} + \bar{}_{m3n}e^{-iq_n y}\right\}e^{-i(E+n!)t} & \text{lead 3; } y < 0 \\ \sum_n \left\{\pm_{m;4}\pm_{n;0}e^{iq_n y} + \bar{}_{m4n}e^{-iq_n y}\right\}e^{-i(E+n!)t} & \text{lead 4; } y < 0. \end{cases} \tag{15}$$

Following similar procedure as in the previous subsection, we can solve for the coefficients. The relation between $\pm^\epsilon$ and $\pm^\epsilon$ is of the same form as in Eq. (12) except that $\epsilon_0 = \epsilon$.

The zero-temperature conductance G is then given by

$$G = \frac{2e^2}{h}\left\{\sum_n \frac{q_n}{q_0}|t_{12n}|^2 + \frac{\left(\sum_n \frac{q_n}{q_0}(|\bar{\jmath}_{13n}|^2 + |\bar{\jmath}_{14n}|^2)\right)\left(\sum_n \frac{q_n}{q_0}(|t_{32n}|^2 + |t_{42n}|^2)\right)}{2 - \sum_n \frac{q_n}{q_0}(|\bar{\jmath}_{33n}|^2 + |\bar{\jmath}_{34n}|^2 + |\bar{\jmath}_{43n}|^2 + |\bar{\jmath}_{44n}|^2)}\right\}. \quad (16)$$

After some algebra, we can simplify the relations to the following form, with

$$\pm^1_i = \frac{1 + (1 - \varepsilon)R}{2 - \varepsilon R}\pm^1; \quad (17)$$

and

$$G = \frac{2e^2}{h}\left\{\frac{(2 - \varepsilon)T}{2 - \varepsilon + \varepsilon T}\right\}. \quad (18)$$

Here R and T are the current reflection and transmission probabilities for the time-modulated potential only. These probabilities are related to the coefficients t_{12n}, but with the coupling parameter $\varepsilon = 0$. In another words, $T = \sum_n (q_n/q_0)|t_{12n}|^2$ and $R = 1 - T$ for $\varepsilon = 0$. Equations (17) and (18) are of the same form as that for elastic scattering. The difference here is that T and R consist of contributions from scattering into various sidebands.

III. Numerical results

In this section, we present numerical examples for the G versus μ characteristics in the presence of both the time-modulated potential and the incoherent scatterings. The results depend on L, V, and ω, which are, respectively, the spatial extent, the amplitude, and the frequency of the time-modulated potential. The results also depend on ε, the coupling parameter of the incoherent scatterer. Our numerical examples can be applied to the case of semiconductors by choosing the energy unit $E^* = 9$ mev, length unit $L^* = 79.6$ Å, and frequency unit $\omega^* = 13.6$ THz.

In Fig. 2, we present the relative shift $(\mu - \mu_r)/\omega$ in the chemical potential of the reservoir μ_r for the case when incoherent processes occur within the time-modulated region. The physical parameters are $\omega = 0.014$, $V = 0.036$, $L = 150$, and $\varepsilon = 0.001$. The curve shows that μ_r maintains only a small deviation from the chemical potential μ of the end-electrodes. This demonstrates that the imposed condition of zero current between the reservoir μ_r and the NC is easily handled by the present model. The oscillations in the curve are found to arise from multiple scatterings that occur within the time-modulated region. Assuming perfect reflections at an edge of the time-modulated region, we can estimate the chemical potentials $\mu = \mu_R$ at which these kind of resonances occur. These resonances occur at $\mu_R(n,m) = n\omega + \left(\frac{m\pi}{L}\right)^2$, for integer values n and m. In fact, even though the values of μ at the peaks in the curve always fall short of the values for $\mu_R(n,m)$, they correspond quite reasonably to the values $\mu_R(0,m)$ for $m = 1,2,3,4,5$; and $\mu_R(1,m)$ for $m = 1,2,3,4,5$. This trend, however, is expected because the actual length for the multiple scattering is longer than L.

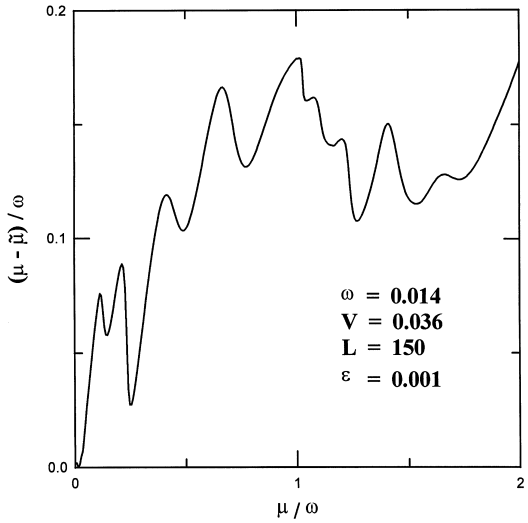

FIG. 2. Relative deviation of the chemical potential ($\mu - \tilde{\mu}$)/$\hbar\omega$ versus $\mu/\hbar\omega$. Physical parameters are $L = 150$, $\hbar\omega = 0.014$, $V = 0.036$, and $\varepsilon = 0.001$. The incoherent processes occur inside the time-modulated region.

In Figs. 3a and 3b, we present the G versus μ characteristics for four values of ε, with $\varepsilon = 0.001$, 0.3, 0.6, and 0.9. The other physical parameters are $\hbar\omega = 0.014$, $V = 0.012$, and $L = 150$. The incoherent processes occur inside, and outside, the time-modulated region in Fig. 3a, and Fig. 3b, respectively. For the $\varepsilon = 0.001$ curve, the transport is essentially coherent and the G characteristics exhibit a dip structure at $\mu/\hbar\omega = 1$. This is the quasibound state feature because the incident electron, with energy $\mu = \hbar\omega$, can make a transition to its subband bottom by emitting an energy $\hbar\omega$ while traversing the time-modulated region [6]. It is then temporarily trapped by the quasibound state formed just below the subband bottom. That there is indeed such a quasibound state can be confirmed by a pole in the current transmission coefficient when the energy μ is allowed to have a small but negative imaginary part [10]. The oscillatory features in G is the harmonic features resulted from multiple scattering of the particle within the time-modulated region. We note in Fig. 3a that as ε increases the harmonic features are suppressed, the dip structure becomes shallower while its width is broadened, and the overall G values are suppressed.

Comparing Figs. 3a and 3b, we see that except for the dip structure and the harmonic features, the numerical values of G for the same ε are fairly close to one another. The conductance for Fig. 3b is given by Eq. (18). By setting $T = 1$, we obtain for the G in Fig. 3b its optimum value for a given ε, which is

$$G = \frac{2e^2}{h}\left(1 - \frac{\varepsilon}{2}\right). \tag{19}$$

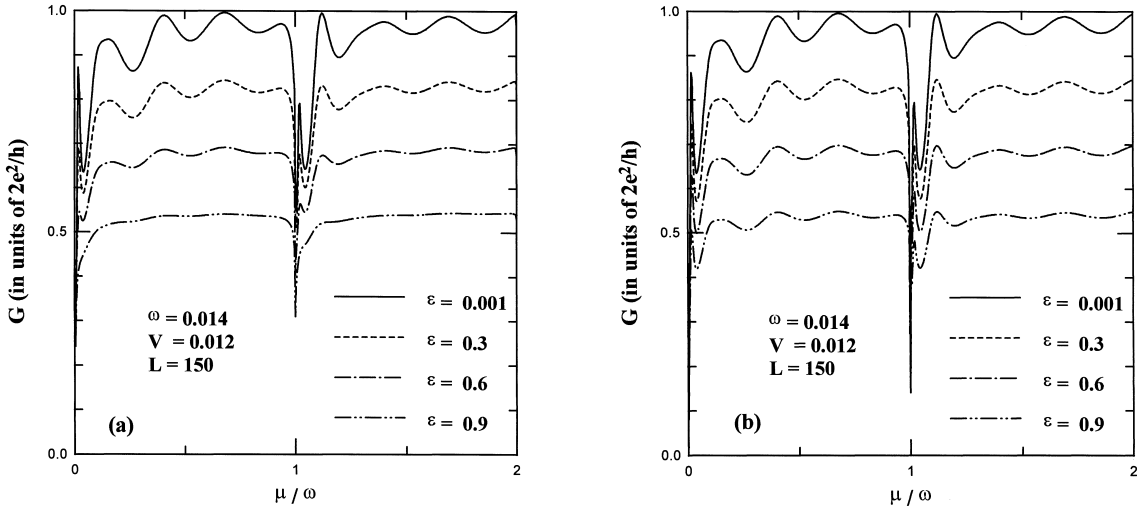

(a) (b)

FIG. 3. Conductance G as a function of ¹ for L = 150, V = 0:012, and ! = 0:014. The coupling parameters " = 0.001, 0.3, 0.6, and 0.9. Fig. 3a is for incoherent processes occuring within the time-modulated region and Fig. 3b is for incoherent processes occuring outside the time-modulated region.

Indeed, the numerical values of G for both of the figures are fairly close to but bounded by that given by Eq. (19). On the other hand, the major difference in the two figures is with the harmonic features. Fig. 3a shows that G suffers strong suppression in the harmonic structures as " increases while Fig. 3b shows only a very mild suppression of the harmonic structures in G. Meanwhile, the dip structure is more prominent in the latter figure. This demonstrates unequivocally that the multiple scattering within the time-modulated region is not affected by the incoherent processes for the case of Fig. 3b. On the contrary, in Fig. 3a, when incoherent processes occur within the time-modulated region, the probability for an electron to traverse coherently from one end to the other end of the region will certainly drop as " increases. The lack of new harmonic features also shows that the introduction of incoherent scatterer does not bring in new coherent multiple scattering length scales. This again illustrates that the incoherent scatterer model has described the incoherent processes appropriately.

In Figs. 4a, 4b, and 4c, we present the G versus ¹ characteristics for L = 100, 150, 200, and for " = 0.3, 0.99. Other physical parameters are ! = 0:014 and V = 0:012. The incoherent processes occur within the time-modulated region in Fig. 4a, and the incoherent processes occur outside the time-modulated region in Fig. 4b and 4c. The dip structure at ¹ = ! persists in all of the curves. This is very important because this demonstrates that the quasibound state feature is very robust against the incoherent processes. In Fig. 4a, even though we have presented the curve for (L; ") = (100; 0.99), our results show that the curves for (L; ") = (150; 0.99) and (200, 0.99) fall exactly onto the (100, 0.99) curve. Therefore, the G characteristics depend on L for " = 0.3 but are independent of L for " = 0.99. In addition, the harmonic features are found in " = 0.3

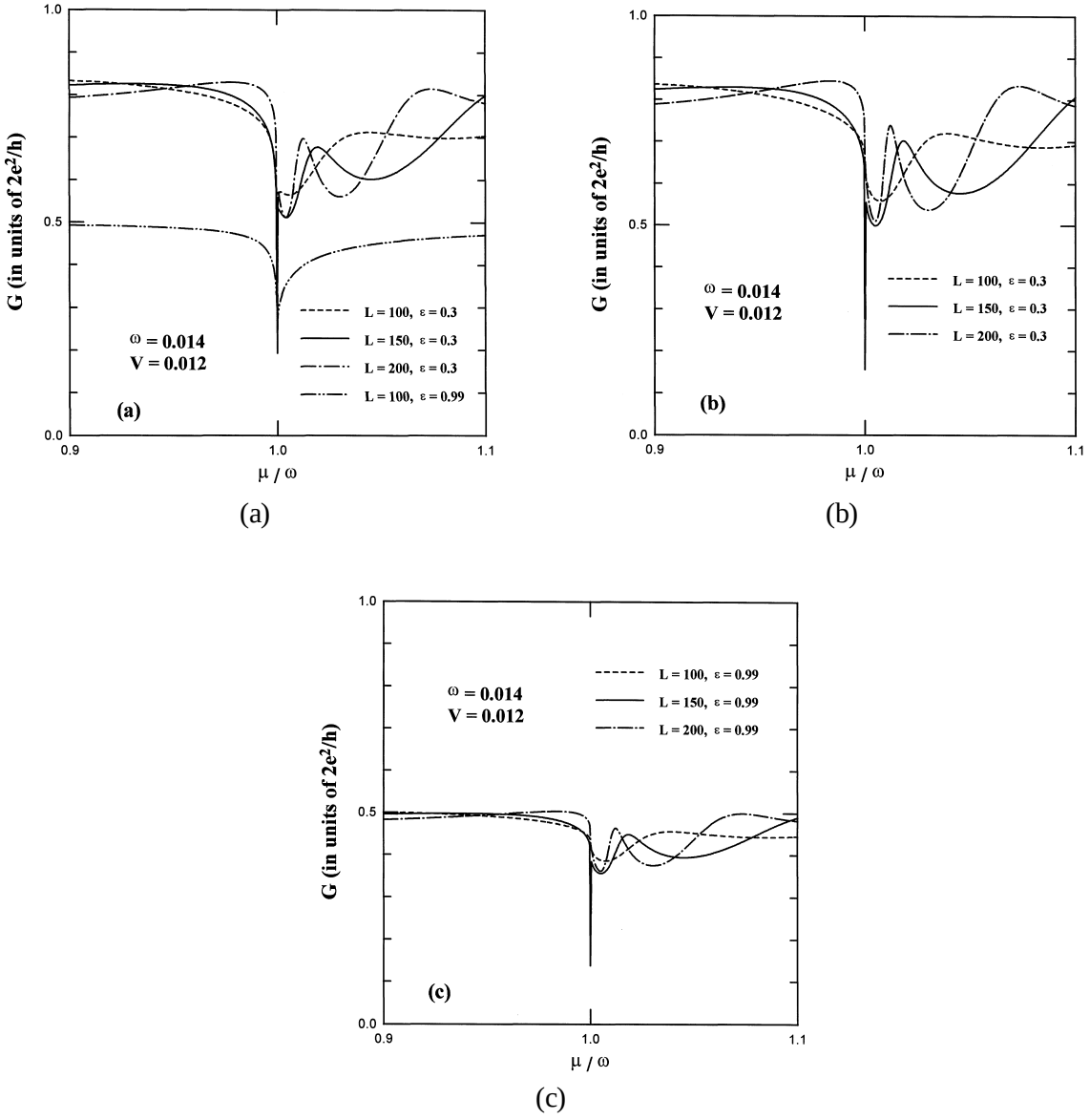

FIG. 4. Conductance G as a function of ¹ for L = 100, 150, and 200. Physical parameters are ! = 0:014, and V = 0:012, and " = 0:3 and 0.99. Fig. 4a is for incoherent processes occuring within the time-modulated region. Figs. 4b, 4c are for incoherent processes occuring outside the time-modulated region.

but vanishes in " = 0.99. These features together show that the electrons can no longer traverse the entire L coherently for " = 0:99. In Figs. 4b and 4c, however, the L dependence and the harmonic features are evident in all curves. Also, the dip structures are more prominent than their counterparts in Fig. 4a. These are consistent with the fact that incoherent processes occurring

outside the time-modulated region contribute only a minimal disruption to the coherent multiple scattering processes that occur inside the region.

IV. Conclusion

In conclusion, we have formulated a theory that treats incoherent processes and coherent inelastic scatterings on the same footing. The theory is cast into a scattering problem which allows us to perform nonperturbative and efficient calculation. We have applied the theory to a simple case of quantum transport through a NC. Our results show that the quasibound state features in G that are induced by the time-modulated potential are very robust against the presence of incoherent processes in the system.

Acknowledgements

This work was partially supported by the National Science Council of the Republic of China through Contract No. NSC 89-2112-M-009-019.

References

[1] B. I. Belevtsev, Yu. F. Komnik, and E. Yu. Beliayev, Phys. Rev. B **58**, 8079 (1998).
[2] B. N. Libenson and V. V. Rumyantsev, Phys. Solid State **40**, 1283 (1998).
[3] J. Rundgren, Phys. Rev. B **59**, 5106 (1999).
[4] P. W. Brouwer and C. W. J. Beenakker, Phys. Rev. B **55**, 4695 (1997).
[5] M. Wagner, Phys. Rev. B **49**, 16544 (1994).
[6] C. S. Tang and C. S. Chu, Phys. Rev. B **53**, 4838 (1996).
[7] B. L. Altshuler, M. E. Gershenson, and I. L. Aleiner, Physica E **3**, 58 (1998).
[8] M. Büttiker, IBM J. Res. Develop. **32**, 63 (1988).
[9] T. P. Pareek, Sandeep K. Joshi, and A. M. Jayannavar, Phys. Rev. B **57**, 8809 (1998).
[10] P. Bagwell and R. K. Lake, Phys. Rev. B **46**, 15329 (1992).